



Construction of Z-scheme type CdS–Au–TiO₂ hollow nanorod arrays with enhanced photocatalytic activity

Haiming Zhu^a, Beifang Yang^{a,*}, Jiao Xu^a, Zhengping Fu^a, Meiwang Wen^a, Ting Guo^a, Shenquan Fu^b, Jian Zuo^b, Shuyuan Zhang^b

^a Department of Materials Science and Engineering, University of Science and Technology of China, Hefei, Anhui 230026, PR China

^b Structure Research Laboratory, University of Science and Technology of China, Hefei, Anhui 230026, PR China

ARTICLE INFO

Article history:

Received 18 December 2008

Received in revised form 2 April 2009

Accepted 4 April 2009

Available online 11 April 2009

Keywords:

Z-scheme

Three-component nanojunction

TiO₂ hollow nanorod arrays

Photocatalytic

Photodeposition

ABSTRACT

The Z-scheme type CdS–Au–TiO₂ hollow nanorod arrays have been constructed on glass substrates by following these simple steps: firstly, highly ordered TiO₂ hollow nanorod arrays (THNAs) were synthesized by liquid phase deposition (LPD) using ZnO nanorod arrays as templates; then both Au core and CdS shell nanoparticles were achieved on the THNAs by in situ photodeposition. The prepared three-component films were characterized by field-emission scanning electron microscopy (FSEM), high-resolution transmission electron microscope (HRTEM), Raman scattering and ultraviolet–visible absorption spectrum. The results showed that Au–CdS core–shell nanoparticles were well dispersed on wall of anatase THNAs from top to bottom. The three-component nanojunction system was evaluated for their photocatalytic activity through the degradation of methylene blue (MB) in aqueous solution. It was found that the CdS–Au–TiO₂ three-component hollow nanorod arrays exhibited significantly enhanced photocatalytic activity compared with single (THNAs) and two components (Au–THNAs or CdS–THNAs) systems. Reasons for this enhanced photocatalytic activity were revealed by photoluminescence (PL) results of our samples.

© 2009 Elsevier B.V. All rights reserved.

1. Introduction

In last few decades, photocatalytic degradation of organic pollutants in waste water using semiconductors nanomaterials has attracted much attention [1]. Owing to high photocatalytic activity, stability and nontoxicity, TiO₂ has been considered as one of the most promising photocatalysts [2–6]. One major limitation of TiO₂ system in photocatalysis is the quick recombination of photoinduced charge carriers [7–9]. To overcome this obstacle, the photocatalysts with various composite structures have been extensively studied. For example, using TiO₂ powder, Tada et al. recently developed an all-solid-state Z-scheme CdS–Au–TiO₂ three-component (3C) nanojunction system [10]. The “Z-scheme system” in the combined structure involves two-step excitation process: it is similar to the photosynthesis process in green plants [11–13]. The Z-scheme 3C nanojunction demonstrated much higher photocatalytic activity than single- (1C) and two-component (2C) systems for the reduction of methylviologen [10]. Tada et al. proved the two-step photo-excitation process in 3C system and ascribed the enhanced photocatalytic performance to

vectorial electron transfer. Yet to date, there are limited reports about the all-solid-state Z-scheme 3C system, and the charge separation effect in this kind of 3C system needs to be further clarified and confirmed.

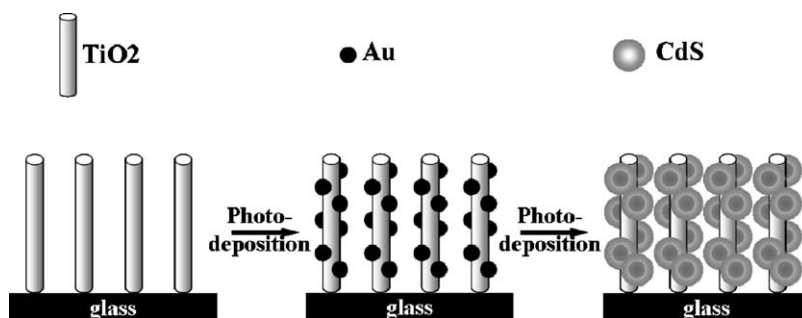
On the other hand, in practical use, obvious drawbacks of TiO₂ powder photocatalyst suspended in solution are the agglomeration and the need of the high costs of the concomitant filtration facilities to recover the catalyst. Therefore, high-efficient photocatalyst system immobilized on substrate is of great significance. TiO₂ photocatalysts in form of thin film [14,15], mesoporous structure [5,16] and so forth have been developed in the last years.

Further more, one-dimension nanostructures arrays on substrates have also attracted much attention because of its efficient light harvesting and photoinduced charge separation [17,18] and great antireflection effect [19] and high specific surface area. The photocatalytic activity of bare TiO₂ hollow nanorod arrays supported on Ti foil has been investigated widely [20–22]. However, limited work has been reported on the TiO₂ hollow nanorod/nanotube arrays-based composite structure [23]. To our knowledge, no report has so far been found regarding TiO₂ one-dimensional arrays-based Z-scheme system.

In the present study, we seek to combine the excellent photocatalytic activity of Z-scheme type system with immobilized TiO₂ one-dimension arrays. Here, we would like to report the

* Corresponding author.

E-mail address: bfiyang@ustc.edu.cn (B. Yang).



Scheme 1. Scheme illustration of the synthesis steps of CdS–Au–THNAs system.

synthesis of CdS–Au–THNAs composite system on glass substrates and the investigation of its photocatalytic activity compared with 1C and 2C systems. In the fabrication methods of TiO₂ one-dimension hollow nanorods arrays, the process of electrochemical anodic oxidation of pure titanium sheet is commonly reported. However, this process requires high cost and the specific substrate. Instead, we chose a facial and low-cost ZnO template solution method reported by Lee et al. [24], which was a one-step method of preparing TiO₂ one-dimensional nanostructure arrays on Si substrate using ZnO nanorod arrays template. In addition, in situ photodeposition is mild in reaction condition and allows the Au core to be selectively loaded at THNAs's reaction sites. This method leads to the greatest possible homogeneous distribution of size-controlled Au core and CdS shell nanoparticles onto the THNAs. Thus the in situ photodeposition procedure was adopted to prepare both Au core and CdS shell nanoparticles. The mechanisms of photocatalytic activity enhancement of the three-component THNAs film were discussed by means of PL measurements results.

2. Experiment

2.1. Sample preparation

The CdS–Au–THNAs three-component sample was prepared by following three steps (Scheme 1): firstly, TiO₂ hollow nanorod arrays (THNAs) on glass substrates were synthesized using a one-step templating liquid phase deposition (LPD) approach reported by Lee et al. [24]. ZnO nanorod arrays using as templates were prepared in a typical two-step method [25]. The glass substrate, which was precasted with ZnO seed layer through sol–gel method [26], was suspended vertically in an aqueous solution of zinc acetate dihydrate (0.021 M) and methenamine (0.021 M) at 363 K for 30 min. After reaction and purification, the glass substrate with ZnO nanorod arrays was immersed vertically in a solution containing 0.05 M ammonium fluorotitanate ((NH₄)₂TiF₆) and 0.15 M boric acid (H₃BO₃) for 3 h at ambient temperature. When ZnO core was etched completely, the THNAs film was obtained. Subsequently, the samples were annealed at 723 K for 3 h in air in order to obtain crystalline TiO₂. Secondly, Au nanoparticles were distributed on TiO₂ hollow nanorod wall by the in situ photo-deposition method [7]. The as-prepared THNAs film was pre-irradiated with UV light (main wavelength: 254 nm, 1.9 mW/cm²) for 3 h to enhance its hydrophilicity [27] and then soaked in 5 mM HAuCl₄ aqueous solution at 333 K for 3 h to allow complete adsorption of AuCl₄[−] ions onto TiO₂ surface. After being rinsed with distilled water and dried in environmental temperature, the film was irradiated with a 20 W low-pressure mercury lamp (main wavelength: 254 nm, 1.9 mW/cm²) for 5 min to reduce adsorbed Au³⁺ to Au nanoparticles and then was washed with distilled water repeatedly to remove the residual AuCl₄[−] totally. Thirdly, the CdS shell layer was selectively coated on the surface of the resulting Au particles also through photocatalytic deposition [10]. The Au-

loaded THNAs sample was immersed in an ethanol solution containing S₈ (1.38 mM) and Cd(NO₃)₂·6H₂O (13.84 mM) and was bubbled with N₂ for 12 h in the dark to remove the dissolved oxygen. Distance from the sample to surface of ethanol solution was fixed to 3 mm. Then UV irradiation was conducted for 7 h under a 20 W low-pressure mercury lamp (wavelength: 320–400 nm; integrated intensity: 0.6 mW/cm²) at room temperature.

CdS–THNAs sample was prepared by chemical bath deposition (CBD) method [28]. THNAs sample was dipped in a 0.5 M Cd(NO₃)₂ ethanol solution for 5 min, rinsing it with ethanol, and then dipping it for another 5 min in a 0.5 M Na₂S methanol solution, and rinsing it with methanol.

2.2. Characterization

The surface morphologies of THNAs films were examined by FSEM (JSM-6700F). HRTEM images and selected area energy dispersive X-ray (EDX) spectrum were obtained on a JEOL-2010 transmission electron microscope coupled with an EDX detector (Oxford). To confirm the crystal phase of TiO₂ and existence of CdS, the Raman spectra measurement was carried out on a confocal laser micro-Raman spectrometer (LABRAM-HR) with a 325 nm He–Cd pump laser. UV–vis absorption spectra were measured by an UV–vis spectrophotometer (Shimadzu UV-2401). PL spectra were recorded using fluorescence spectrophotometer (Hitachi F-4600) with xenon lamp as excitation source (λ_{ex} = 360.0 nm) at room temperature. Valence state of elements were analyzed by X-ray photoelectron spectroscopy (XPS) (Thermo Electron ESCALAB-250).

2.3. Photocatalytic measurement

To preclude the influence of surface area on photocatalytic activity, samples for photocatalytic test were of same thickness and geometric area (2 cm × 2 cm). Methylene blue (MB) was employed as a representative dye pollutant to evaluate the photocatalytic activity. After the samples had been immersed in 60 mL of a 10 mg/L MB aqueous solution for 1.5 h to ensure that the products reached adsorption equilibrium, photodegradation of MB in aqueous solution was carried out under UV light irradiation using a 20 W low-pressure mercury lamp (main wavelength: 254 nm, 1.9 mW/cm²) at ambient conditions. The solution was stirred continuously during the whole process. The concentration of reduced MB in each sample was estimated using its maximum absorbance at 664 nm from UV–vis absorption spectrum measured after irradiation for a definite time.

3. Results and discussion

3.1. Catalyst characterization

In the LPD reaction solution, the mixed (NH₄)₂TiF₆ and H₃BO₃ produce TiO₂ and H⁺ ions through hydrolysis reactions. The

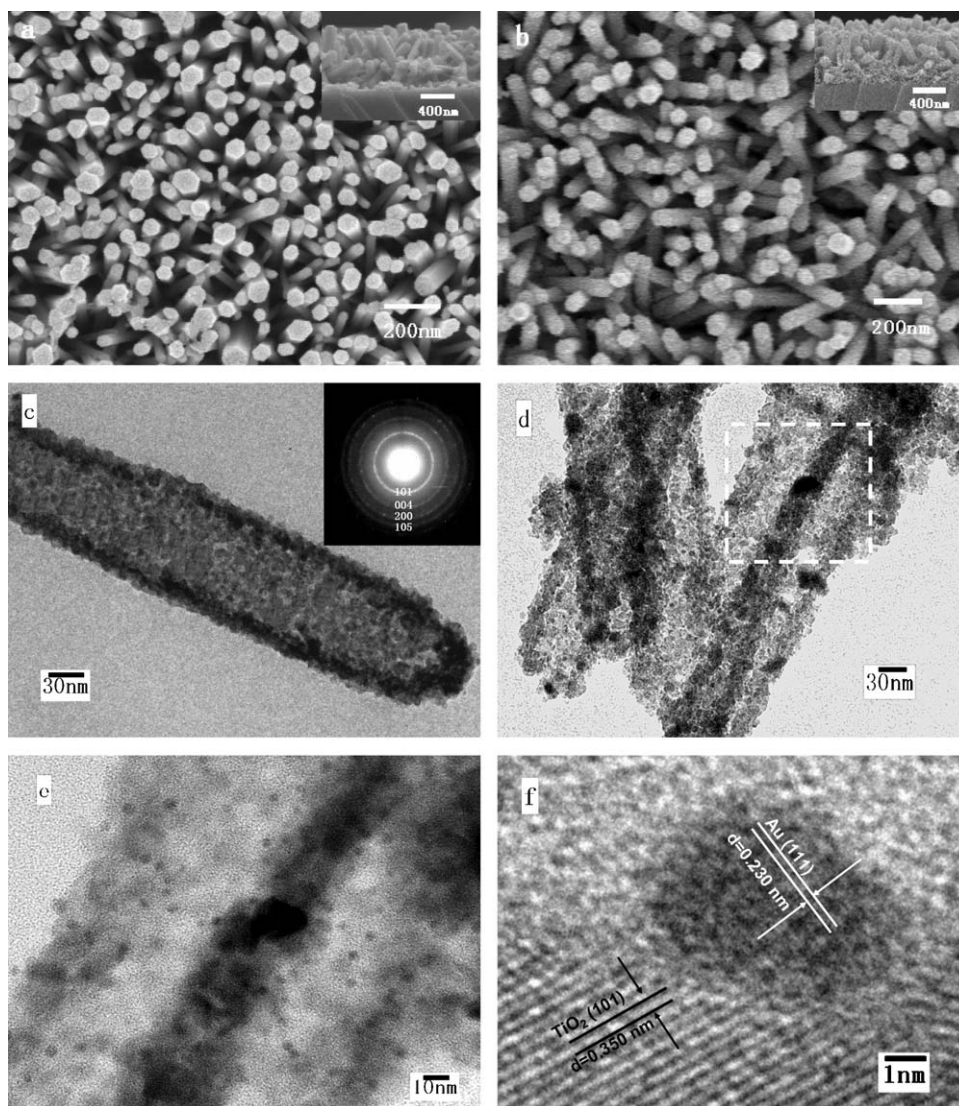


Fig. 1. (a) FSEM image of the well aligned ZnO nanorod arrays template (inset: its cross section); (b) FSEM image of the well aligned THNAs prepared by liquid phase deposition (LPD) using ZnO nanorod arrays as templates in (a) (inset: its cross section); (c) TEM image of as-prepared TiO₂ hollow nanorod (inset: its selected area electron diffraction patterns); (d) low magnification TEM image of Au-loaded TiO₂ hollow nanorod; (e) high magnification TEM image of the Au-loaded TiO₂ hollow nanorod; (f) HRTEM image of Au-loaded TiO₂.

deposition of TiO₂ accompanies the selective etching of ZnO template by H⁺. When all ZnO nanorods are etched out, TiO₂ hollow nanorod structure are formed [24]. Fig. 1(a) shows a typical SEM image of surface morphology of as-synthesized highly oriented ZnO nanorod arrays grown on the entire glass substrate. The ZnO nanorods have an average diameter of ~60 nm and length of ~660 nm. After the formation of the ZnO template, the sample was immersed in the reaction solution for LPD process. According to the Ref. [24], the reaction time was fixed to 3 h to form the TiO₂ hollow nanorod arrays. The morphology of obtained THNAs in Fig. 1(b) shows well aligned TiO₂ nanorod arrays of about 90 nm in diameter and 700 nm in length on glass substrate. Fig. 1(c) is a typical TEM image of as-prepared TiO₂ nanorod, revealing that the TiO₂ nanorod has a hollow and end-closed structure with a wall thickness of about 15 nm. The detailed formation mechanism of the TiO₂ hollow nanorod arrays was raised in Ref. [24]. The deposited structure was composed of TiO₂ nanoparticles and exhibited a polycrystalline structure as shown by the selected-area electron diffraction rings in Fig. 1(c) inset. Four well-resolved Raman peaks in Fig. 4(a) are observed at 147, 398, 519 and 641 cm⁻¹, corresponding to the characteristic Raman modes of anatase TiO₂.

Photodeposition of Au nanoparticles on resulting THNAs was carried out under UV light irradiation after adsorption in HAuCl₄ aqueous solution. The density and size of Au nanoparticles loaded on TiO₂ hollow nanorods could be controlled by changing the adsorption time in HAuCl₄ solution and irradiation time (see [Supplementary material Fig. S1](#)). The Au particle size greatly affects its catalytic performance. It was reported that the Au particles with diameter under 5 nm exhibited unusually high catalytic activity [8,29]. Tada and co-workers demonstrated that Au nanoparticles on TiO₂ could reduce S₈ to S²⁻ and the reduction ability increased with decreasing Au particle size [30]. To efficiently coat CdS layer on Au, we chose the Au particle of smaller size and higher density for further research. Fig. 1(d) is a low magnification TEM image of the as-synthesized Au-loaded TiO₂ sample and Fig. 1(e) is a higher-magnification TEM image of selected area marked in Fig. 1(d). These images show that dense and ultrafine Au nanoparticles have been well dispersed on the entire wall of TiO₂ hollow nanorods from top to bottom. The average size of Au nanoparticles is 4.5 nm with narrow size distribution (Fig. 2; based on TEM observation). The observed lattice fringes spacing of 0.230 and 0.350 nm in Au–TiO₂ HRTEM image (Fig. 1f) corresponds to the (1 1 1) plane of Au

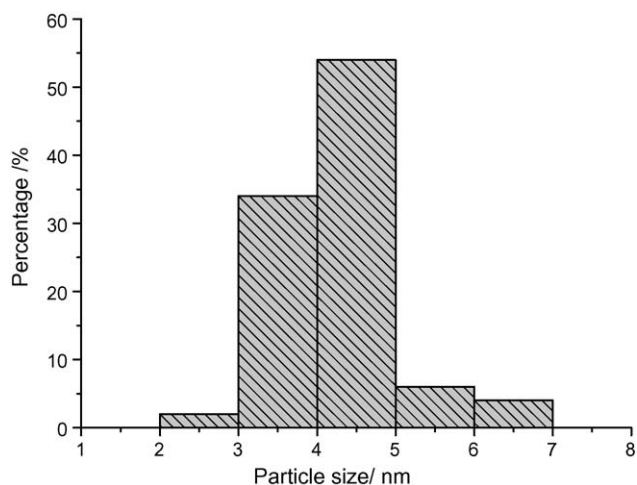


Fig. 2. Particle size distribution histograms of Au loaded on TiO₂ hollow nanorod.

and (1 0 1) plane of anatase TiO₂, respectively (JCPDS-ICDD 89-3697 and 89-4203). The deposited metallic Au is also verified by XPS result (see Supplementary material Fig. S2).

After the as-prepared Au-THNAs sample was immersed in ethanol solution containing S₈ and Cd(NO₃)₂·6H₂O and irradiated with UV light, S₈ was reduced to S²⁻ by the photoinduced electrons that were agglomerated on Au. Meanwhile Cd²⁺ in the solution bonded to S²⁻ to form hemispherical CdS layer coated on the Au nanoparticles. The high disperse degree of Au nanoparticles on TiO₂ hollow nanorods led to the well-dispersed Au (core)–CdS (shell) nanoparticles. The thickness of CdS layer could be controlled by the irradiation time [10]. Fig. 3(a) inset is a typical TEM image of as-synthesized CdS–Au–TiO₂ 3C sample after 7-h reaction in our experiment. Although the CdS coating could not be clearly resolved from the top view because of its overlap with Au and TiO₂, the spatial hybrid structure may be easily seen from the side wall. From the TEM image, the average thickness of CdS shell is about 4 nm. The observed lattice fringes spacing in HRTEM image (Fig. 3(a)) (see Supplementary material Fig. S3); focusing on one particle area marked in Fig. 3(a) inset) 0.352, 0.230 and 0.319 nm, agree with the (1 0 1) plane of anatase TiO₂, (1 1 1) plane of Au and (1 0 1) plane of hexagonal CdS (JCPDS-ICDD 89-2944), respectively, which confirm the Au (core)–CdS (shell) nanoparticles well loaded on TiO₂ surface. The micro-area EDX (Fig. 3(b)) of the sample area in Fig. 3(a) reveals the chemical composition of as-prepared 3C sample. The Cd and S elements were detected and the Cd/S atomic ratio was analyzed to be 1:0.76. CdS nanocrystals synthesized in

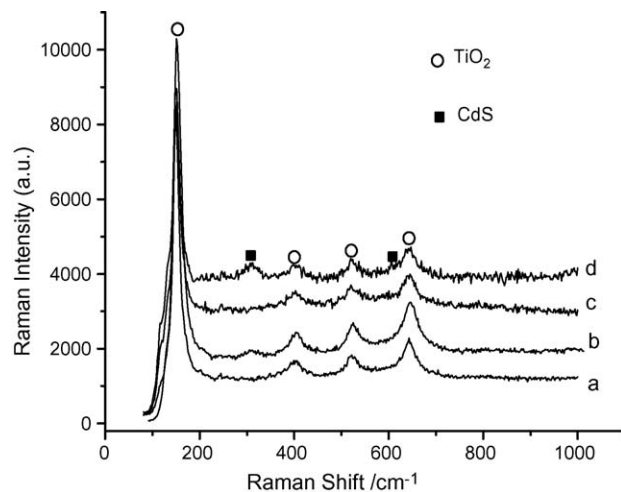


Fig. 4. Raman spectra of (a) pure THNAs annealed in air at 723 K for 3 h; (b) CdS-THNAs; (c) Au-THNAs; and (d) CdS–Au-THNAs.

liquid phase most often show an excess of Cd²⁺ relative to S²⁻ [31]. Compared with pure THNAs and Au-THNAs, the 3C sample's Raman spectrum in Fig. 4(d) yields peaks at 306 and 604 cm⁻¹, which are in agreement with the longitudinal optical phonon mode (1LO) of CdS lattice and the overtone of this mode (2LO) reported in Ref. [32]. The Raman spectrum confirms the formation and presence of CdS in as-prepared 3C system.

In CdS-THNAs 2C system for comparison, the formation of CdS on THNAs through CBD was also confirmed by the Raman spectrum in Fig. 4(b).

Fig. 5 gives the UV–vis absorption spectra of (a) pure THNAs and (b) CdS-THNAs, (c) Au-THNAs, (d) CdS–Au-THNAs multicomponent systems, respectively. All the samples are of same thickness and size. For pure THNAs, the strong absorption at wavelength range below 400 nm is due to the intrinsic interband transition absorption of pure anatase TiO₂. The absorption of pure THNAs in visible region can be assigned to scattering of light caused by pores or cracks in the nanorod arrays [33,34]. Compared with pure THNAs, Au-THNAs composite shows a broad peak at 530 nm, corresponding to plasmon resonance (PR) absorption of Au nanoparticles. The peak position and shape are consistent with those of 5 nm Au particles loaded on TiO₂ reported in Ref. [8]. After deposited CdS shell on Au nanoparticles, the PR absorption peak of Au nanoparticles redshifted to ~585 nm and broadened due to the strong electromagnetic coupling of Au and CdS [35]. The shoulder peak at 430 nm of 3C system is due to the absorption of CdS shell.

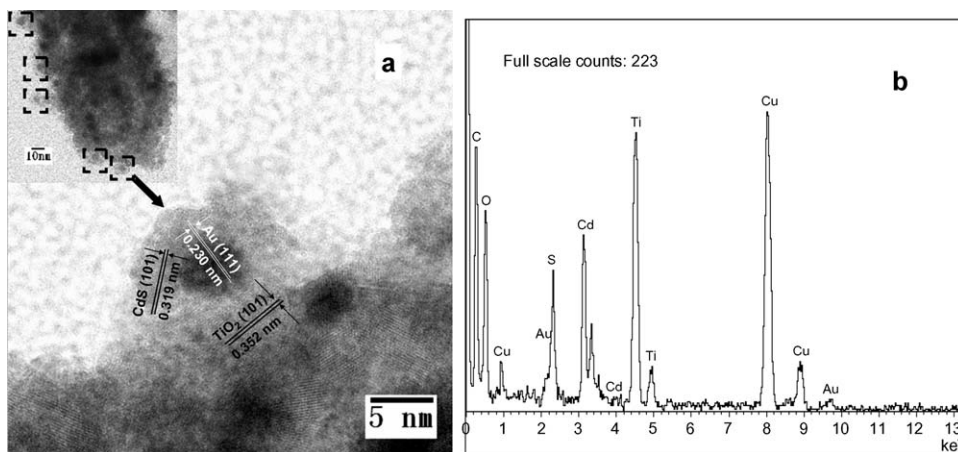


Fig. 3. HRTEM image of CdS–Au-THNAs (a); and corresponding EDX result (b). Inset in (a) is the 3C sample's TEM image under low magnification.

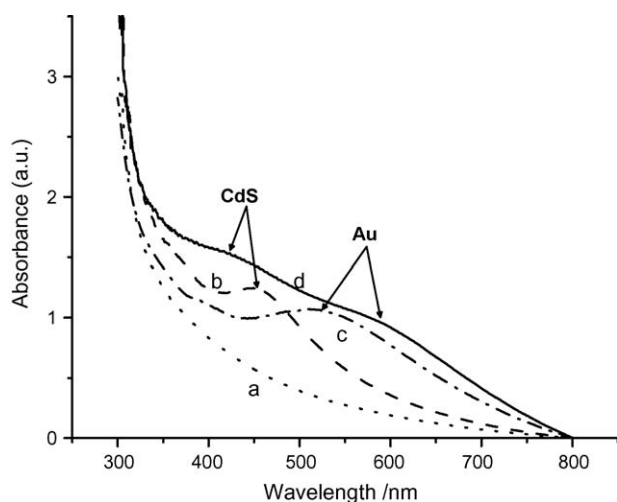


Fig. 5. UV-vis absorption spectra of (a) pure THNAs; (b) CdS-THNAs; (c) Au-THNAs; and (d) CdS-Au-THNAs.

From calculation with the effective-mass approximation [36], which gives relationship between ground-state exciton absorption energy and particle diameter, the thickness of the CdS shell is estimated to be ~ 4 nm. The estimated thickness is consistent with the TEM image result. The average size of CdS nanoparticles in CdS-THNAs 2C sample for comparison is determined to be ~ 6.5 nm from its 452 nm absorption peak.

3.2. Photocatalytic activity

The samples were first immersed in 60 mL of a 10 mg/L MB aqueous solution for 1.5 h to ensure that the products reached adsorption equilibrium (see [Supplementary material Fig. S4](#)), and then photodegradation of MB under UV light irradiation was performed in order to evaluate the photocatalytic activity of prepared CdS-Au-THNAs three-component composites. Photocatalysis of pure THNAs, Au-THNAs and CdS-THNAs were also tested for comparison. A typical time-evolved photodecomposition curve is shown in [Fig. 6](#). After adsorption of 90 min, the whole reaction system reached adsorption equilibrium. Using pure THNAs as a photocatalyst, the concentration of MB was only reduced by about 15% after 120 min irradiation. CdS-THNAs and Au-THNAs two-component nanojunctions show higher photolysis activity, the concentration of MB was reduced by about 25% and 35%,

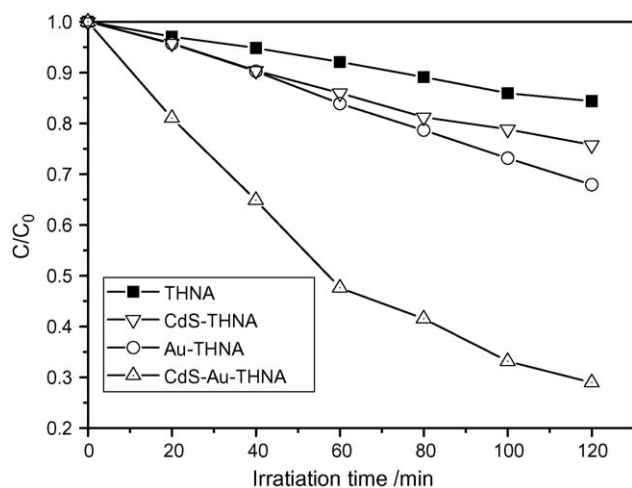


Fig. 6. Time courses for photocatalytic degradation of methylene blue under UV light irradiation on pure THNAs, CdS-THNAs, Au-THNAs, CdS-Au-THNAs catalysts.

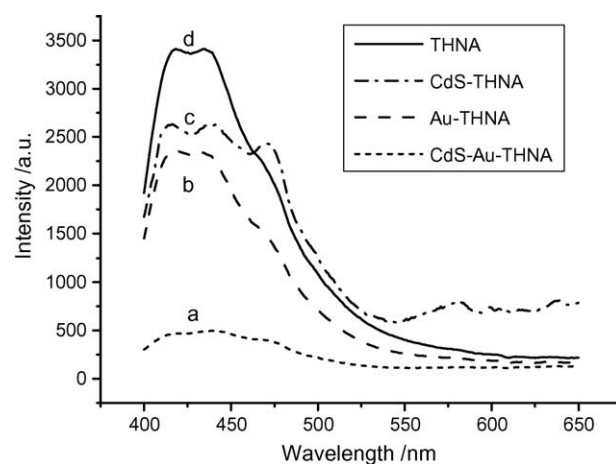


Fig. 7. Room temperature photoluminescence spectrum of (a) CdS-Au-THNAs; (b) Au-THNAs; (c) CdS-THNAs; and (d) THNAs (xenon lamp as excitation source, $\lambda = 360$ nm).

respectively. Compared with the single- and the two-component systems, the CdS-Au-THNAs three-component nanojunction exhibited marked enhanced photocatalytic activity, the concentration of MB was reduced by about 72% after the same time irradiation.

3.3. Mechanism of the enhancement of the photocatalytic activity

Photocatalytic activity is closely related with the lifetime of photogenerated electrons and holes. PL signals result from the recombination of photoinduced charge carriers [37]. To confirm the charge separation behavior and efficiency in 3C system, we carried out PL measurements by a spectrophotometer containing a xenon lamp with 360 nm excitation wavelength. Let us compare the PL spectra ([Fig. 7](#)) for as-prepared 3C system and single- and two-component systems. All the samples displayed a broad-band emission from 400 to 500 nm with similar three peaks: 417, 439 and 471 nm. Usually, the origin of the PL spectrum of anatase TiO_2 materials can be divided into three kinds: self-trapped excitons [38], oxygen vacancies [39] and surface states [40]. In our samples, the prominent peak position of the 417 nm band is very close to that in [Ref. \[41\]](#) (421 nm) and [Ref. \[42\]](#) (425 nm). Moreover, its position did not change with Au or CdS deposition, indicating that this band probably originated from the intrinsic states rather than the surface states. So the 417 nm band should be attributed to radiative recombination of self-trapped excitons localized on TiO_6 octahedra. PL bands at longer wavelength of anatase TiO_2 have been attributed to oxygen vacancies [39]. Shallow oxygen vacancies trap levels at 0.41 eV (444 nm) [39] and 0.57 eV (472 nm) [41] below conduction band have been ascertained and established. Pure THNAs, Au-THNAs and CdS-Au-THNAs give only a non-distinctive shoulder peak at 472 nm, but for CdS- TiO_2 2C system, it shows a relatively high intensity. Considering emission character of solution-synthesized CdS and quantum size effect, the enhancement was presumably due to the superposition of CdS's green emission band from trap states. For CdS nanocrystals synthesized in aqueous solutions, these trap states have been attributed to surface stoichiometric excesses of Cd^{2+} . As already noted above, the micro-area EDX spectra for as-prepared 3C sample show an excess of Cd^{2+} relative to S^{2-} [31,43].

It is generally believed that a lower excitonic PL intensity means an enhanced separation and transfer of photoinduced electrons trapped in TiO_2 [37]. From the PL results, CdS-THNAs and

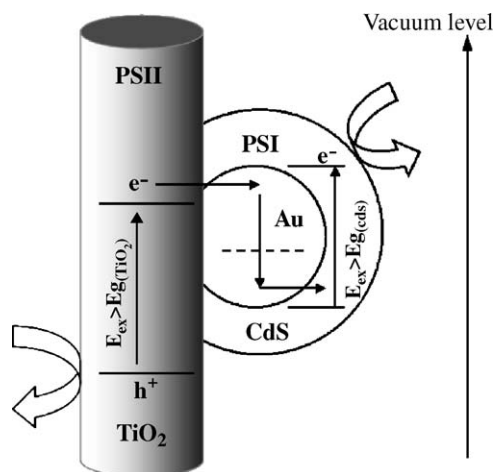


Fig. 8. Charge transfer mechanism in the Z-scheme type 3C photocatalyst using Au as mediator.

Au-THNAs 2C system exhibited diminished PL intensity indicating reduced charge recombination compared with pure THNAs. For CdS–Au-THNAs 3C system, drastic quenching of PL intensity suggests a markedly enhanced charge separation than single- and two-component systems.

In 2C system, due to the photoinduced electron injection from CdS into the conduction band of attached TiO₂ particles for CdS-THNAs [44], the transfer of electrons from TiO₂ to gold nanoparticle for Au-THNAs [8], higher charge separation can be obtained. So 2C systems exhibit higher photocatalytic performance than pure THNAs. However, the photocatalytic activity of both 1C and 2C systems was far lower than CdS–Au–TiO₂ 3C system. The charge migration mechanism should be similar to that proposed by Tada et al. [10]. Through a two-step excitation of CdS (PSI), TiO₂ (PSII) and with Au as a mediator, which is similar to Z-scheme in green plants' photosynthesis, photoinduced electrons achieve a vectorial transfer of TiO₂ → Au → CdS in such three-component system (Fig. 8).

Considering the mechanism in Fig. 8, accumulation of photoinduced electrons in PSI (CdS) and holes in PSII (TiO₂) by the electron-transfer system Au (indicated as black narrow arrow), are spatially separated. Thus, the reduction on PSI surface and the oxidation on PSII surface (indicated as white wide arrow) are also spatially separated. However, these two roles vectorially superposed to a resultant force which continuously drives the photoinduced charge carriers. Holes remained on TiO₂ valence-band and electrons concentrated on CdS conduction-band, respectively, which enabled the Z-scheme type 3C system strong oxidation and reduction capabilities. Furthermore, the PL results herein confirmed that the vectorial electrons transfer in such Z-scheme type 3C system greatly improves the separation rate of photo-induced charges. Thus the UV-light photocatalytic activity of three-component systems far exceeded that of the single (THNAs) and two-component (Au-THNAs or CdS-THNAs) systems.

4. Conclusions

By facile photodeposition method, highly ordered TiO₂ hollow nanorod arrays on glass substrates were successfully co-modified with Au (core) and CdS (shell) nanoparticles. Compared with 1C and 2C systems, the Z-scheme type 3C system exhibited a notable enhanced photocatalytic activity. The enhancement resulted from the strong oxidation/reduction abilities and the high photoinduced charge separation

efficiency. The charge separation effect was confirmed by PL results. In addition, further study on anionic doping of THNAs is needed to improve the visible photoresponse of the Z-scheme type CdS–Au–TiO₂ hollow nanorod arrays [4].

Acknowledgement

This work is supported by China National Natural Science Research Foundation.

Appendix A. Supplementary data

Supplementary data associated with this article can be found, in the online version, at doi:10.1016/j.apcatb.2009.04.006.

References

- [1] M.R. Hoffmann, S.T. Martin, W.Y. Choi, D.W. Bahnemann, *Chemical Reviews* 95 (1995) 69–96.
- [2] A.L. Linsebigler, G.Q. Lu, J.T. Yates, *Chemical Reviews* 95 (1995) 735–758.
- [3] X. Chen, S.S. Mao, *Chemical Reviews* 107 (2007) 2891–2959.
- [4] R. Asahi, T. Morikawa, T. Ohwaki, K. Aoki, Y. Taga, *Science* 293 (2001) 269–271.
- [5] X. Wang, J.C. Yu, C. Ho, Y. Hou, X. Fu, *Langmuir* 21 (2005) 2552–2559.
- [6] Y. Bessekhouad, D. Robert, J. Weber, *Journal of Photochemistry and Photobiology A: Chemistry* 163 (2004) 569–580.
- [7] B. Kraeutler, A.J. Bard, *Journal of the American Chemical Society* 100 (1978) 4317.
- [8] V. Subramanian, E.E. Wolf, P.V. Kamat, *Journal of the American Chemical Society* 126 (2004) 4943–4950.
- [9] M.A. Fox, M.T. Dulay, *Chemical Reviews* 93 (1993) 341–357.
- [10] H. Tada, T. Mitsui, T. Kiyonaga, T. Akita, K. Tanaka, *Nature Materials* 5 (2006) 782–786.
- [11] R. Hill, F. Bendall, *Nature* 186 (1960) 136–137.
- [12] H. Kato, M. Hori, R. Kenta, Y. Shimodaira, A. Kudo, *Chemistry Letters* 33 (2004) 1348–1349.
- [13] J. Barber, *Nature* 376 (1995) 388–389.
- [14] H. Yamashita, M. Honda, M. Harada, Y. Ichihashi, M. Anpo, *Journal of Physical Chemistry B* 102 (1998) 10707–10711.
- [15] I.M. Arabatzis, T. Stergiopoulos, M.C. Bernard, D. Labou, S.G. Neophytides, P. Falaras, *Applied Catalysis B: Environmental* 42 (2003) 187–201.
- [16] J.L.L. Chen, G.v. Freymann, S.Y. Choi, V. Kitaev, G.A. Ozin, *Advanced Materials* 18 (2006) 1915–1919.
- [17] O.K. Varghese, M. Paulose, K. Shankar, G.K. Mor, C.A. Grimes, *Journal of Nanoscience and Nanotechnology* 5 (2005) 1158–1165.
- [18] W. Lee, J. Lee, S. Lee, W. Yi, S.-H. Han, B.W. Cho, *Applied Physics Letters* 92 (2008) 153510.
- [19] Y.J. Lee, D.S. Ruby, D.W. Peters, B.B. McKenzie, J.W.P. Hsu, *Nano Letters* 8 (2008) 1501–1505.
- [20] G.K. Mor, K. Shankar, M. Paulose, O.K. Varghese, C.A. Grimes, *Nano Letters* 5 (2005) 191–195.
- [21] Q. Xie, S.G. Yang, X.L. Ruan, H.M. Zhao, *Environmental Science and Technology* 39 (2005) 3770–3775.
- [22] Z. Liu, X. Zhang, S. Nishimoto, M. Jin, D.A. Tryk, T. Murakami, A. Fujishima, *Journal of Physical Chemistry C* 112 (2008) 253–259.
- [23] S.G. Chen, M. Paulose, C. Ruan, G.K. Mor, O.K. Varghese, D. Kozoudis, C.A. Grimes, *Journal of Photochemistry and Photobiology A: Chemistry* 177 (2006) 177–184.
- [24] J.-H. Lee, I.-C. Leu, M.-C. Hsu, Y.-W. Chung, M.-H. Hon, *Journal of Physical Chemistry B* 109 (2005) 13056–13059.
- [25] L.E. Greene, M. Law, J. Goldberger, F. Kim, J.C. Johnson, Y.F. Zhang, R.J. Saykally, P.D. Yang, *Angewandte Chemie International Edition* 42 (2003) 3031–3034.
- [26] M. Ohyama, H. Kozuka, T. Yoko, *Thin Solid Films* 306 (1997) 78–85.
- [27] X. Feng, J. Zhai, L. Jiang, *Angewandte Chemie International Edition* 44 (2005) 5115–5118.
- [28] C.H. Chang, Y.L. Lee, *Applied Physics Letters* 91 (2007) 053503.
- [29] M. Haruta, *Catalysis Today* 36 (1997) 153–166.
- [30] T. Kiyonaga, T. Mitsui, M. Torikoshi, M. Takekawa, T. Soejima, H. Tada, *Journal of Physical Chemistry B* 110 (2006) 10771–10778.
- [31] S. Gorer, J.A. Ganske, J.C. Hemminger, R.M. Penner, *Journal of the American Chemical Society* 120 (1998) 9584–9593.
- [32] D.S. Chu, C.M. Dai, W.F. Hsieh, C.T. Tsai, *Journal of Applied Physics* 69 (1991) 8402–8404.
- [33] J.G. Yu, H.G. Yu, B. Cheng, X.J. Zhao, J.C. Yu, W.K. Ho, *Journal of Physical Chemistry B* 107 (2003) 13871–13879.
- [34] J.G. Yu, X.J. Zhao, Q.N. Zhao, *Thin Solid Films* 379 (2000) 7–14.
- [35] I. Honma, T. Sano, H. Komiyama, *Journal of Physical Chemistry* 97 (1993) 6692–6695.
- [36] P.E. Lippens, M. Lannoo, *Physical Review B* 39 (1989) 10935–10942.
- [37] L.Q. Jing, Y.C. Qu, B.Q. Wang, S.D. Li, B.J. Jiang, L.B. Yang, W. Fu, H.G. Fu, J.Z. Sun, *Solar Energy Materials and Solar Cells* 90 (2006) 1773–1787.

- [38] H. Tang, H. Berger, P.E. Schmid, F. Levy, G. Burri, *Solid State Communications* 87 (1993) 847–850.
- [39] N. Serpone, D. Lawless, R. Khairutdinov, *Journal of Physical Chemistry* 99 (1995) 16646–16654.
- [40] W.F. Zhang, M.S. Zhang, Z. Yin, Q. Chen, *Applied Physics B: Lasers and Optics* 70 (2000) 261–265.
- [41] X.F. Song, L. Gao, *Langmuir* 23 (2007) 11850–11856.
- [42] Y. Lei, L.D. Zhang, G.W. Meng, G.H. Li, X.Y. Zhang, C.H. Liang, W. Chen, S.X. Wang, *Applied Physics Letters* 78 (2001) 1125–1127.
- [43] O. Demelo, L. Hernandez, O. Zelayaangel, R. Lozadamorales, M. Becerril, E. Vasco, *Applied Physics Letters* 65 (1994) 1278–1280.
- [44] L. Spanhel, H. Weller, A. Henglein, *Journal of the American Chemical Society* 109 (1987) 6632–6635.